JOURNAL OF CATALYSIS **161,** 790–797 (1996)
ARTICLE NO. 0242

Hydrodechlorination of Carbon Tetrachloride over Pt/MgO

Hyun Chul Choi, Sun Hee Choi, O Bong Yang,[1] Jae Sung Lee, Kyung Hee Lee,[2] and Young Gul Kim

Department of Chemical Engineering, Pohang University of Science and Technology (POSTECH), San 31 Hyoja-dong, Pohang, 790-784 Korea

Received December 22, 1995; revised March 13, 1996; accepted March 18, 1996

Hydrodechlorination of carbon tetrachloride (CCl_4) has been studied at various reaction temperatures, mole ratios (H_2/CCl_4), and WHSVs over 1% Pt/MgO. The main factors determining conversion of CCl_4 and deactivation of the catalyst were reaction temperature and H_2/CCl_4 mole ratio. The optimum reaction conditions for obtaining stable and high conversions of CCl_4 above 90% were the reaction temperature of 413 K, H_2/CCl_4 mole ratio of 9, and WHSV of 9000 liters/kg/h. The surface area of catalyst decreased due to phase change of MgO to $MgCl_2 \cdot xH_2O$ during reaction. Relative to fresh catalyst, the amounts of carbon and chlorine increased and that of oxygen decreased in used catalyst, especially in deactivated catalyst. The catalyst used for the steady-state reaction did not chemisorb H_2 at room temperature, but chemisorbed nearly the same amounts of H_2 as those observed for the fresh catalyst at 373 K. From the XPS and XAFS measurements the active phase of Pt during hydrodechlorination appeared to be a surface Pt(II) species with Cl ligands, while the bulk remained as Pt metal.

INTRODUCTION

Carbon tetrachloride (CTC) is a versatile chemical used as a reagent and a solvent in chemical industry and as a source of carbon dopant on semiconductors and for etching Ga–As microchips in the semiconductor industry (1, 2). Yet it was classified as a material of Group IV among ozone-depleting chlorofluorocarbons (CFCs) at the Fourth Copenhagen conference in 1992. Thus the use of CTC will be banned in developed countries from 1996. Therefore, development of an efficient method to dispose of it is in order.

Three methods have been used to dispose of CFCs including CTC: thermal combustion (3, 4), catalytic combustion (5), and catalytic hydrogenation (6, 7). Thermal combustion is an energy-consuming process because a combustion temperature above 1200 K is required and the process produces secondary pollutants such as dioxins. The catalytic combustion over Pt is also an energy-consuming process requiring a temperature between 700 and 800 K and produces secondary pollutants such as CO, Cl_2, or $COCl_2$. Catalytic hydrogenation over noble metals is desirable because the reaction temperature is usually between 380 and 480 K and useful products like chloroform ($CHCl_3$) or dichloromethane (CH_2Cl_2) are produced. Hence, the hydrodechlorination of CTC has been actively studied, particularly in industrial laboratories since the 1990s. (8–13). In addition to these disposal methods, nonconventional radiolytic, electrochemical, or biological methods have also been proposed (14, 15).

In hydrogenation of CTC, Vance and Bauman (16) studied the reaction of atomic hydrogen and CTC ($H + CCl_4 \rightarrow CCl_3 + HCl$) in 1938 and obtained a steric factor of 0.007 and activation energy of 3.45 kcal/mol in a gas-phase reaction by the classical bimolecular reaction theory.

Weiss *et al*. (6, 17) studied the hydrogenation of CTC over Pt/η-Al_2O_3 and Ni ion-exchanged Y-type zeolite (NiY). The experimental results over Pt/η-Al_2O_3 showed selective hydrogenation of CTC to $CHCl_3$ and CH_4. The reactivity of the products, $CHCl_3$, CH_2Cl_2, and CH_3Cl, was below 10% of the reactivity of CTC. The authors proposed that the reaction of CTC with H_2 over the Pt/η-Al_2O_3 catalyst proceeded via two parallel routes, producing $CHCl_3$ and CH_4 at a constant mole ratio independent of process variables. Namely, the formation of $CCl_3\cdot$ radical is the initiation step and hydrogen addition to adsorbed $CCl_3\cdot$ accounts for $CHCl_3$ and the concerted Cl abstraction, and hydrogen addition to $CCl_3\cdot$ with no important desorption of intermediates accounts for CH_4. Over NiY, C_2 ($C_2Cl_2H_4$, $C_2Cl_4H_2$, and C_2Cl_6) and C_3 ($C_3Cl_2H_6$) products were produced by oligomerization of free radicals.

In our previous work (18), we studied the effects of various supports (γ-Al_2O_3, SiO_2, MgO, TiO_2, SiO_2–Al_2O_3, ZrO_2, NaY) in Pt-catalyzed hydrodechlorination of CTC For 1 wt% Pt loading accomplished by impregnation with a H_2PtCl_6 solution, MgO was found to be the most stable support against catalyst deactivation. ln the present paper, the effects of various reaction conditions such as reaction temperature, space velocity and mole ratio of H_2/CTC have been studied in the hydrodechlorination of CTC over the 1% Pt/MgO catalyst. Various analytical methods (X-ray diffraction, X-ray photospectroscopy, H_2 chemisorption, X-ray absorption fine structure) were employed in order

[1] Present address: Chonbuk National University, Chonju, 560-756, Korea.

[2] To whom correspondence should be addressed. Fax: 82-0562-279-5799.

0021-9517/96 $18.00

to identify the active phase of Pt during the reaction and to understand the cause of catalyst deactivation.

EXPERIMENTAL

Hexachloroplatinic acid ($H_2PtCl_6 \cdot xH_2O$, Aldrich, purity >99.9%) was used as a precursor to the catalysts. MgO was prepared from the decomposition of $Mg(OH)_2$ (Aldrich, purity >95%) at 773 K in air. The resulting MgO (surface area, 170 ± 5 m^2 g^{-1}; pore volume, 1.1 ± 0.1 ml g^{-1}) was impregnated with a hexachloroplatinic acid solution. After drying for 24 h at 383 K, the sample was calcined in oxygen flow (>99.99%) for 2 h at increasing temperatures up to 573 K (heating rate, 5 K min^{-1}) and reduced in hydrogen flow (>99.99%) for 2 h at increasing temperatures up to 573 K (heating rate, 5 K min^{-1}). The platinum loading was 1.0 wt%, and the content of Pt in the catalysts was confirmed to be 1.0 ± 0.02 wt% by inductively coupled plasma–atomic emission spectroscopy.

The chemisorption of hydrogen was carried out in a conventional volumetric adsorption apparatus at room temperature (RT) in the pressure range of 10–70 kPa. The sample was first reduced *in situ* under hydrogen flow at 573 K for 2 h and then evacuated to 1×10^{-5} Pa at 673 K for 1 h. The sample was cooled to RT and the first H_2 chemisorption isotherm was taken. The sample was then evacuated to 1×10^{-5} Pa at RT, and the second isotherm was taken. The linear part of two isotherms was extrapolated to zero pressure. The amount of chemisorbed H_2 was the difference of two isotherms at zero pressure. The particle size d_p of Pt was estimated from the H_2 chemisorption data assuming spherical Pt particles (19).

The size of the metallic particles was also checked by transmission electron microscopy (TEM) using a JEOL 200CX microscope.

The N_2 BET surface area, S_g, was measured in a conventional volumetric adsorption apparatus (Micrometrics Accusorb 2100E) at liquid nitrogen temperature. X-ray diffraction (XRD) experiments were carried out with a Rigaku Dmax-B diffractometer with Cu$K\alpha$ radiation. X-ray photospectroscopy (XPS) spectra was recorded using a PHI 5400 ECSA spectrometer employing Mg$K\alpha$ source ($h\nu = 1253.6$ eV). The binding energy of C_{1s} at 284.6 eV for contaminated carbon was used as the reference for the binding energy calibration.

X-ray absorption fine structure (XAFS) experiments were performed on the beam lines 7C and 10B at the Photon Factory in the National Laboratory for High Energy Physics, Tsukuba, Japan. The samples were pressed into thin self-supporting wafers of 8 mm diameter and mounted in a Pyrex *in situ* spectroscopic cell with Kapton windows where the sample would be treated under different gas flows and temperatures. Spectra of the Pt L_{III} edge were recorded at room temperature after reduction and reaction for the samples still under the atmosphere of treating gases in the cell. In addition to catalyst samples, XAFS data were also obtained for Pt foil, $PtCl_2$, $PtCl_4$, and PtO_2 samples as references. XAFS data were analyzed by the UWXAFS 2.0 package and FEFF6 code licensed from the University of Washington (20, 21).

The selective hydrogenation of CTC was carried out in a continuous isothermal flow reactor fitted with a glass frit on which 200 mg of catalyst was placed. The reaction temperature ranged from 393 to 453 K, and the molar ratio of the reactants (H_2/CTC), from 5 to 15. The weight hourly space velocity (WHSV, liters CTC/kg catalyst/h) was kept at 9000 liters/kg/h except when the effect of WHSV was tested. Liquid CTC was vaporized in a saturator by flowing hydrogen as a carrier gas. The temperature of the reactor was controlled by a PID temperature controller within ±1 K and the temperature of the saturator was controlled by a circulating bath within ±0.1 K. The effluent from reactor was analyzed by on-line gas chromatography (HP 5890 II) with a capillary column (AT-1, 30 m × 0.3 mm i.d.) and a flame ionization detector. The conversion of CTC and selectivity to $CHCl_3$ were defined as

$$\text{Conversion of CTC (\%)} = \frac{\text{moles CTC in} - \text{moles CTC out}}{\text{moles CTC in}} \times 100$$

$$\text{Selectivity to } CHCl_3 \text{ (\%)} = \frac{\text{moles } CHCl_3 \text{ out}}{\text{moles CTC in} - \text{moles CTC out}} \times 100$$

RESULTS

Hydrodechlorination of CTC

Figure 1 shows the change in the conversion of CTC with time on stream at reaction temperatures in the range of 393–453 K at a constant WHSV of 9000 liters/kg/h and mole ratio (H_2/CTC) of 9. At 393 K, the conversion of CTC was only 20%, but the stable conversion of CTC was observed with respect to time on stream. Above 433 K, the initial conversion of CTC was high, but the conversion decreased rapidly with time on stream. The deactivation was more severe at 453 K than at 433 K. Furthermore, more C_2 or heavier products were produced at higher reaction temperatures. High and stable catalytic activity was obtained at 413 K. It is interesting to note that CTC conversions increased in the initial several hours before it reached steady states at 393 and 413 K.

The effects of the mole ratio of reactants (H_2/CTC) were investigated at 413 K and WHSV of 9000 liters/kg/h and the results are shown in Fig. 2. At H_2/CTC ratio of 5, the catalyst was rapidly deactivated. Above H_2/CTC ratio of

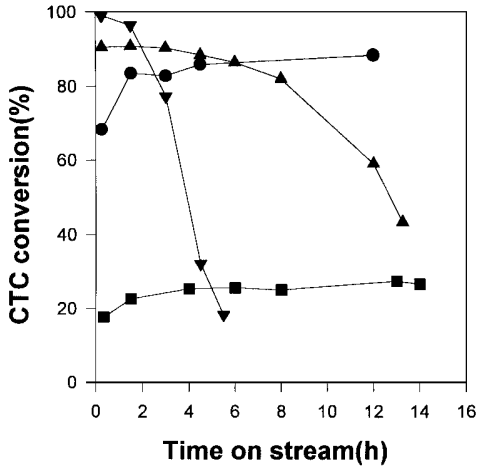

FIG. 1. Effects of reaction temperature on hydrodechlorination of CTC at atmospheric pressure, H_2/CTC mole ratio of 9, and WHSV of 9000 liters/kg/h. ■, 393 K; ●, 413 K; ▲, 433 K; ▼, 453 K.

9, stability of the catalyst was achieved and the conversion of CTC was independent of the mole ratio. The effects of WHSV were tested by varying flow rate of reactants or the weight of the catalyst at 413 K and H_2/CTC ratio of 9. As shown in Fig. 3, CTC conversion decreased as WHSV increased. The selectivity to $CHCl_3$ showed a slight decrease with increasing WHSV. At 413 K, H_2/CTC ratio of 9, and WHSV of 9000, CTC conversion above 95% and $CHCl_3$ selectivity of ca. 70% were obtained.

Typical product distributions of CTC hydrodechlorination over 1% Pt/MgO are shown in Table 1. In all cases, $CHCl_3$ and CH_4 were the main products, and small amounts of CH_2Cl_2 and CH_3Cl were observed at steady state. C_2 and heavier oligomers were produced for the worst cases early in the reaction but disappeared almost completely at steady state under favorable conditions. Yet, a high reaction temperature (above 433 K) or a low H_2/CTC mole ratio showed high C_2 selectivity. In particular, 34% C_2 selectivity was measured at 453 K, H_2/CTC ratio of 9, and WHSV of 9000. As WHSV was increased, $CHCl_3$ selectivity decreased because of the increased CH_4 selectivity, but C_2 selectivity was independent of WHSV.

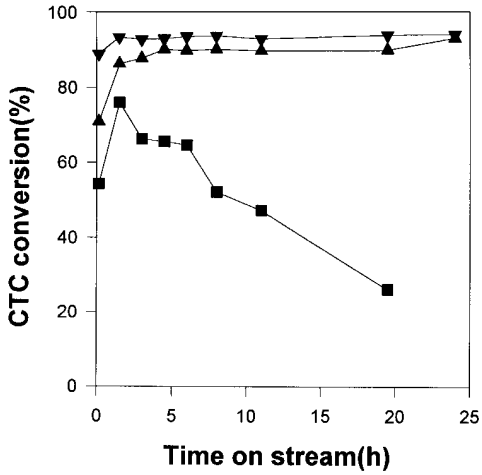

FIG. 2. Effects of H_2/CTC mole ratio on hydrodechlorination of CTC at 413 K and WHSV of 9000 liters/kg/h. ■, 5/l; ▲, 9/l; ▼, 15/l.

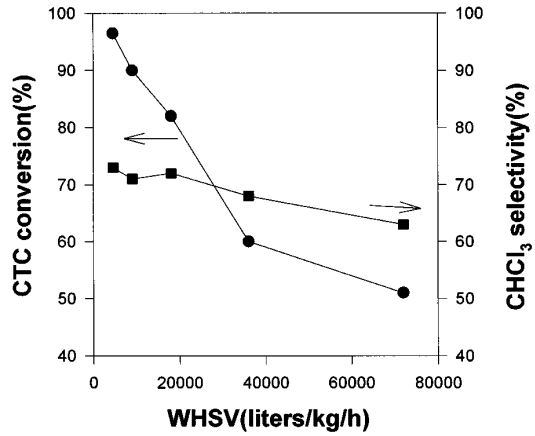

FIG. 3. Effects of WHSV on hydrodechlorination of CTC at 413 K and H_2/CTC mole ratio of 9.

Catalyst Characterization

Some results of characterization are summarized in Table 2. The BET surface area, S_g, of 1% Pt/MgO was found to be 169 $m^2\ g^{-1}$. This is the same area measured for MgO support alone. The catalyst used for the steady-state reaction at 413 K, H_2/CTC of 9, and WHSV of 9000 for 80 h (called *used catalyst* hereafter) showed an S_g of 48 $m^2\ g^{-1}$. The catalyst used for the reaction at 453 K, H_2/CTC of 9, and WHSV of 9000 for 10 h showed severe catalyst deactivation and will be called *deactivated catalyst* hereafter. The deactivated catalyst showed an S_g value of 45 $m^2\ g^{-1}$.

The hydrogen adsorption was carried out at RT. The percentage of Pt exposed to the surface and particle size of platinum were deduced from the amounts of H_2 chemisorbed. In the fresh 1% Pt/MgO, 50% Pt was exposed (0.5 H/Pt) and Pt particle size was calculated to be 1.8 nm from this value. The used catalyst showed no hydrogen uptake at RT, but showed nearly the same amount of hydrogen uptake as that of the fresh catalyst when hydrogen chemisorption was measured at 373 K. Deactivated catalyst did not show any H_2 chemisorption at both RT and 373 K.

The TEM images of the 1% Pt/MgO revealed a homogeneous distribution of platinum particles. The mean particle diameter d_m, was calculated by the equation $d_m = \Sigma n_i d_i / \Sigma n_i$, where n_i is the number of particles of diameter d_i. The platinum particle sizes determined by TEM were ca. 2.0 nm for fresh, used, and deactivated 1% Pt/MgO. The size and shape of Pt particles remained almost the same in all catalyst.

TABLE 1

Typical Product Distribution of Hydrodechlorination of Carbon Tetrachloride over 1% Pt/MgO[a]

T(K)	413	393	433[b]	453[b]	413[b]	413	413	413
H_2/CTC	9	9	9	9	5	15	9	9
WHSV	9000	9000	9000	9000	9000	9000	4500	70,000
CTC conversion (%)	90	27	88	32	66	93.5	96	52
Products (mole%)								
$CHCl_3$	71	64	60	35	64	75	73	64
CH_4	27.5	30	32	30	25	23.5	25	34
CH_2Cl_2, $CHCl_3$	0.5	0.5	1	1	1	0.5	1	1
C_2	1	5.5	7	34	10	1	1	1
Specific rate (CTC mol/Pt mol/sec)	0.243	0.072	0.236	0.086	0.280	0.142	0.129	4.02

[a] At steady state unless otherwise specified.
[b] At time on stream of 4.5 h.

Table 2 also shows the results of the chemical analysis for the three catalysts. The amounts of carbon in both fresh and used catalysts were almost the same. Yet deactivated catalysts contained much more carbon. Chlorine analysis indicated that the catalysts had picked up chlorine during the reaction. However, there was no difference between used and deactivated catalysts in chlorine content.

Figure 4 compares the XRD pattern of the used (Fig. 4a) 1% Pt/MgO catalyst with those of the fresh catalyst (Fig. 4b) and $MgCl_2 \cdot 6H_2O$ (Fig. 4c). Because of the low contents and small particle size of platinum metal, the XRD peaks for platinum metal were not observed. MgO was the dominant phase in the fresh catalyst. On the other hand, used catalyst showed both $MgCl_2 \cdot xH_2O$ and MgO phase, indicating that the transformation from MgO to $MgCl_2 \cdot xH_2O$ had occurred during the reaction.

Figure 5 shows the XPS spectra of platinum $4f_{7/2}$ for fresh (Fig. 5a) and used (Fig. 5b) 1% Pt/MgO. Fresh catalyst reduced in H_2 flow at 573 K for 2 h showed a dominant peak at 71.2 eV and a small peak at 73.0 eV corresponding to Pt(0) and Pt(II), respectively. In used catalyst, Pt(II) at 73.2 eV was the dominant species with only a small concentration of Pt(0) at 71.2 eV. Thus, the Pt(0) species initially present on the surface of 1% Pt/MgO catalyst was oxidized to Pt(II) during the reaction.

Table 3 shows the atomic concentration of C, O, and Cl in fresh, used, and deactivated 1% Pt/MgO determined by XPS analysis. As XPS is a surface sensitive technique, the atomic concentration of C, O, and Cl is different from the results of the chemical analysis shown in Table 2. The atomic concentration of C and Cl increased remarkably after the reaction. In particular, C concentration of deactivated catalyst was much higher than used catalyst. This trend in XPS analysis is consistent with that observed by chemical analysis. The atomic concentration of O decreased probably because of a phase transition of support from MgO to $MgCl_2 \cdot xH_2O$, as indicated by XRD.

ln order to obtain further information on the state and structure of Pt in Pt/MgO catalyst, the technique of XAFS was employed. Figure 6 compares Pt L_{III} X-ray absorption near edge structure (XANES) of fresh (Fig. 6a), used

TABLE 2

Characterization Results of 1% Pt/MgO

	Fresh	Used	Deactivated
BET surface area ($m^2\ g^{-1}$)	169	48	45
Particle size (nm)[a]			
From H_2 chemisorption at RT	1.8	2.0[b]	—
From TEM	2.0	2.0	2.0
Chemical analysis (wt%)			
C	0.12	0.10	0.70
Cl	0.05	1.66	1.75

[a] $d_p = 5 \times V_M/a_M \times 100/D$ (%), D (%) = 100 × chemisorbed H/total Pt atoms, where V_M is volume/Pt, a_M is area/Pt atom, and D (%) is the percentage of atoms exposed of the surface measured by the H_2 chemisorption, respectively.
[b] H_2 chemisorption at 373 K.

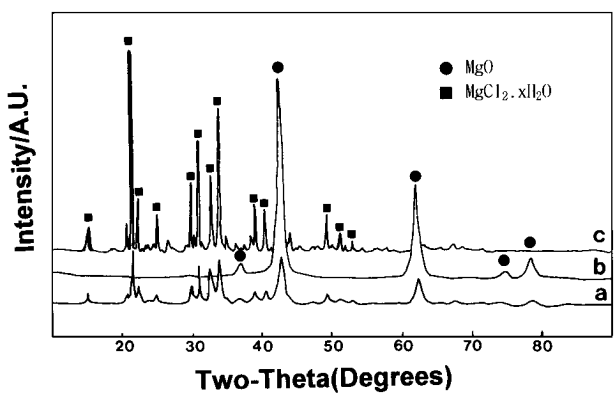

FIG. 4. XRD patterns of 1% Pt/MgO under steady state (a), in fresh state (b), and $MgCl_2 \cdot xH_2O$ (c).

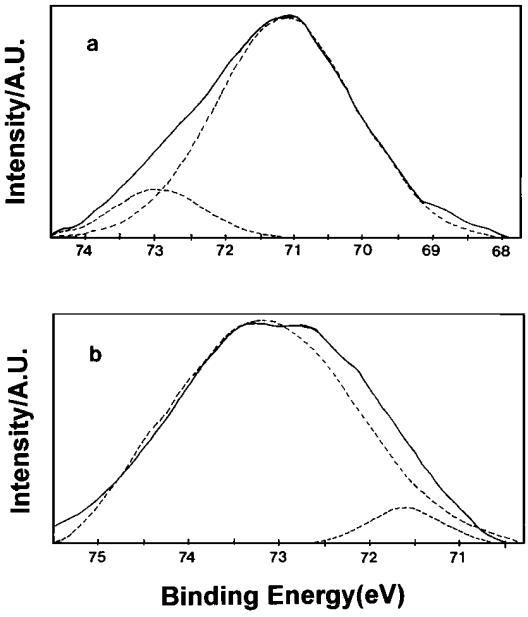

FIG. 5. XPS spectra of 1% Pt/MgO in fresh state (a) and under steady-state reaction (b). Dotted lines are deconvolution of the experimental spectra (solid lines) assuming that Pt(0) and Pt(II) are the only Pt species present in the catalyst.

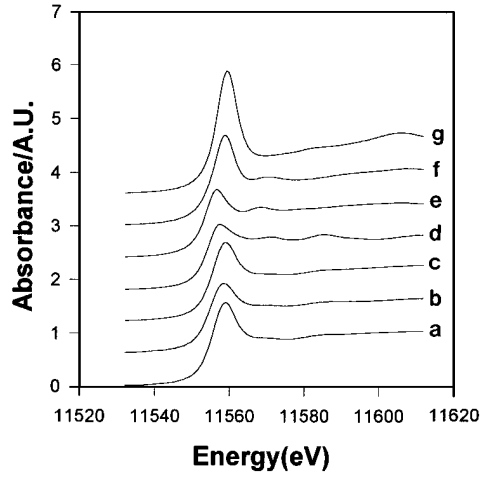

FIG. 6. XANES spectra of Pt L_{III} edge. (a) fresh Pt/MgO; (b) used Pt/MgO; (c) deactivated Pt/MgO; (d) Pt foil; (e) $PtCl_2$; (f) $PtCl_4$; and (g) PtO_2.

(Fig. 6b), and deactivated (Fig. 6c) catalysts with those of some reference compounds, Pt foil (Fig. 6d), $PtCl_2$ (Fig. 6e), $PtCl_4$ (Fig. 6f), and PtO_2 (Fig. 6g). General shape of XANES spectra was all similar. However, the edge position (the first inflection point on the rapidly rising portion of the absorption edge) and white line area (the intensity of the absorption peak) depended on the sample. The quantitative results are summarized in Table 4. In general, the edge position shifts to higher energy and the white line area increases as the oxidation number of the absorption is raised (22–26).

The edge positions of all catalyst samples were higher than those of Pt foil and $PtCl_2$, and lower than those of $PtCl_4$ and PtO_2. A similar trend was observed for white line areas as well. White line areas for catalyst samples were larger than those for Pt foil and $PtCl_2$, and smaller than those for $PtCl_4$ and PtO_2. Hence, the oxidation state of Pt in catalyst samples is also believed to lie between those of the two groups of reference compounds.

Small oscillations above the absorption edge are isolated from the background absorption. This extended X-ray absorption fine structure (EXAFS) is weighted $k^3(k/A^{-1} =$ wave factor) and Fourier transformed to obtain a radial structure function (RSF). Major peaks in the RSF correspond to the important interatomic distances shifted from their true position by a phase shift. The RSF of reference compounds, Pt foil, $PtCl_2$, $PtCl_4$, and PtO_2 are shown in Figs. 7a–7d, respectively. The main peaks correspond to distances of Pt–Pt (0.267 nm in Fig. 7a), Pt–Cl (0.190 nm in Fig. 7b and 7c), and Pt–O (0.163 nm in Fig. 7d). Phase shifts for those atomic pairs could be calculated from the difference between these distances and the known true distance for these compounds.

Figure 8 shows the RSF of catalyst samples. In the fresh Pt/MgO, three peaks appeared at 0.199, 0.274, and 0.371 nm (all in the error range of ±0.0005 nm) as shown in Fig. 8a. In comparison with the RSF of the reference compounds in Fig. 7, the peak at 0.199 nm can be assigned to Pt–Cl of $PtCl_x$

TABLE 3

Atomic Concentration (%) of C, Cl, and O in 1% Pt/MgO by XPS

	Fresh	Used	Deactivated
C[a]	0	7.83	11.74
Cl[b]	3.07	14.89	16.97
O[c]	42.85	30.97	28.97

[a] From C_{1s} peak with a sensitivity factor of 0.296.
[b] From Cl_{2p} peak with a sensitivity factor of 0.891.
[c] From O_{1s} peak with a sensitivity factor of 0.711.

TABLE 4

The Edge Position and White Line Area of Pt L_{III} XANES

Sample	Edge position (eV)	White line area[a]
Fresh catalyst	11555.70	1.25138
Used catalyst	11554.83	1.14038
Deactivated catalyst	11555.50	1.24385
Pt foil	11554.39	1
$PtCl_2$	11553.87	1.05073
$PtCl_4$	11556.15	1.28908
PtO_2	11556.81	2.0044

[a] Relative white line area ($A_{sample}/A_{Pt\,metal}$).

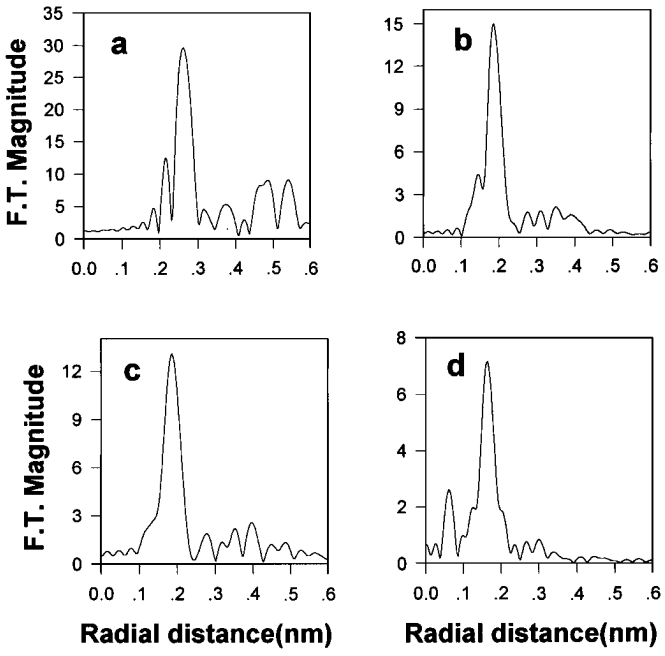

FIG. 7. RSF of references. (a) Pt foil; (b) $PtCl_2$; (c) $PtCl_4$; and (d) PtO_2.

and the peak at 0.274 nm to Pt–Pt in bulk Pt metal. The peak at 0.371 nm is due to the Pt–Pt interaction between neighboring $PtCl_x$ complexes as has been observed for $PtCl_6^{-2}$ (27). Thus Pt remains only partially reduced even after calcination and reduction at 573 K, and retains Cl originated from the precursor $H_2PtCl_6 \cdot xH_2O$.

The RSF of Pt/MgO used for the steady-state reaction also showed three dominant peaks at 0.166, 0.212, and 0.281 nm as shown in Fig. 7b. The peak that appeared at 0.371 nm in fresh catalyst disappeared completely and the peak at 0.166 nm appear. The peak at 0.212 nm seemed related to the peak at 0.199 nm on fresh catalyst assigned to Pt–Cl, and the peak at 0.281 nm could be assigned to Pt–Pt. The peak at 0.166 nm appeared to be due to Pt–O similar to that distance in the PtO_2 reference. Hence, the Pt particle under the steady-state reaction seems to be composed of surface $PtCl_x$, bulk Pt metal, and some PtO_x. The RSF of

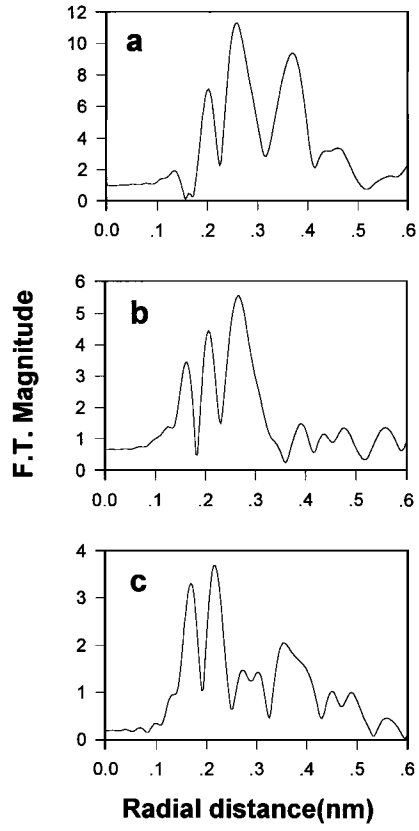

FIG. 8. RSF of 1% Pt/MgO. (a) fresh catalyst; (b) used catalyst; and (c) deactivated catalyst.

the deactivated catalyst showed two main peaks at 0.166 and 0.218 nm which could be assigned to Pt–O and Pt–Cl, respectively. The peak at 0.273 nm expected for Pt–Pt was very small. In general, the intensity of all the peaks decreased from the fresh catalyst to used catalyst and then to deactivated catalyst. Table 5 summarizes the results of EXAFS curve fitting for the Pt–Pt interaction. The Pt–Pt distances increased for the used and deactivated catalysts probably due to the effect of Cl or O near Pt. The values of the coordination numbers and Debye–Waller factors are also given.

TABLE 5

Results of EXAFS Curve Fitting for the Pt–Pt Interaction in 1% Pt/MgO and Pt Foil

	Pt–Pt distance (nm)	Pt coordination number	Debye–Waller factor[a]
Fresh catalyst	0.274	4.4	0.001448
Used catalyst	0.281	4.3	0.001164
Deactivated catalyst	0.285	0.4	0.006465
Pt foil	0.278	12.0	0.004987

[a] Relative to Pt foil, i.e., $\Delta\sigma^2$ (sample)-$\Delta\sigma^2$ (Pt foil).

DISCUSSION

The following four reactions can take place during catalytic hydrodechlorination of CTC.

	ΔH° (kcal/mol) at 400 K	ΔG° (kcal/mol) at 400 K	
$CCl_4 + H_2 \rightarrow CHCl_3 + HCl$	−24.21	−27.74	[1]
$CCl_4 + 2H_2 \rightarrow CH_2Cl_2 + 2HCl$	−44.80	−50.87	[2]
$CCl_4 + 3H_2 \rightarrow CH_3Cl + 3HCl$	−64.30	−72.00	[3]
$CCl_4 + 4H_2 \rightarrow CH_4 + 4HCl$	−84.41	−92.71	[4]

The large negative values of ΔG° (28) indicated that CTC could convert completely to $CHCl_3$, CH_2Cl_2, CH_3Cl, or CH_4. Indeed, almost a complete CTC conversion was observed in the present study under appropriate reaction conditions. Reactions leading to the formation of $CHCl_3$ and CH_4 were dominant as also reported by Weiss *et al.* (6). Oligomers were observed particularly early in the reaction, yet their concentration was negligible at steady state if proper reaction conditions were chosen. Substantial amounts of C_2 products were observed over Ni ion-exchanged Y-type zeolite by Weiss *et al.* (17), probably due to the acidity of the zeolite.

The present work demonstrated that Pt/MgO could be an efficient catalyst for the selective hydrodechlorination of CCl_4 to $CHCl_3$. The most important parameter of the reaction was the stability of the catalyst against the loss of catalytic activity with time on stream. Reaction temperature and the ratio of H_2/CTC were the two critical reaction variables that controlled the catalyst stability. The very reason why we chose Pt/MgO was also its superior stability compared to other supported Pt catalysts (18). In any case, a stable CTC conversion above 95% and $CHCl_3$ selectivity of ca. 70% were achieved at 413 K, H_2/CTC ratio of 9, and WHSV of 9000. The major by-product was methane. As mentioned, Weiss *et al.* (6) proposed that $CHCl_3$ and CH_4 were produced via two parallel routes over the Pt/η-Al_2O_3 catalyst. This appears to be the case for Pt/MgO as well because the $CHCl_3$ selectivity depended only a little over a wide range of WHSV as shown in Fig. 3 and Table 1. If the hydrodechlorination was a consecutive reaction such as $CCl_4 \rightarrow CHCl_3 \rightarrow CH_4$, the selectivity to the intermediate $CHCl_3$ would have been increased with increasing WHSV. Instead, $CHCl_3$ selectivity decreased slightly with increasing WHSV. Furthermore, when $CHCl_3$ was supplied over Pt/MgO under the same conditions, its reactivity was only about 10% of CCl_4. Negligible desorption of intermediates containing one to two chlorine atoms (6) accounts for the low concentrations of these intermediate products.

The XRD in Fig. 4 indicates that MgO support is transformed to $MgCl_2$ during hydrodechlorination. This change in support structure, however, does not appear to be responsible for the catalyst deactivation. Despite the change in support, the particle size of Pt remained essentially the same as seen by TEM (Table 2). Hydrogen chemisorption becomes an activated process over the used catalyst probably because of the presence of Cl on Pt as discussed later. Yet, total amount of chemisorbed H_2 at 373 K over the used catalyst is essentially the same as that over the fresh catalyst at RT. Furthermore, the chlorine content in the deactivated catalyst was almost the same as that in the used catalyst for which no sign of deactivation was detected. Hence, the presence of chlorine is not the cause of the catalyst deactivation. It is believed that the Pt catalyst is deactivated due to coking in the hydrodechlorination of CTC as also proposed by Wang *et al.* (29). Both the chemical analysis in Table 2 and the XPS analysis in Table 3 demonstrated that the content of carbon is the major difference between the used and the deactivated catalysts. Propensity to coking at high temperatures and low H_2/CTC ratios explains the effects of the reaction temperature and H_2/CTC ratio shown in Figs. 1 and 2. It was also found that the deactivated catalyst could be regenerated by oxygen treatment at 573 K for 3 h.

Explanation of Table 1 indicates that the deactivation of Pt/MgO in the hydrodechlorination of CTC goes hand in hand with enhanced production of C_2 products. Thus substantial amounts of C_2 products are formed at high reaction temperatures and low H_2/CTC ratios where rapid catalyst deactivation is observed. The boiling point of C_2Cl_4 is 394 K and that of C_2Cl_6 459.8 K. Thus, it is highly plausible to assume that high boiling oligomers (C_2 and heavier) are the precursors to coke formed on Pt/MgO catalyst.

In order to investigate the active Pt phase, XPS and XAFS were employed. Since XPS is a surface-sensitive technique with a probing depth of ca. 2–4 nm and XAFS is a bulk technique, the combination of the two techniques is expected to provide more detailed structural information on Pt/MgO. XPS of the fresh catalyst (Fig. 5a) showed two binding states of Pt $4f_{7/2}$ at 71.2 and 73.0 eV. The former binding state was dominant and assigned to Pt(0) species and the latter was assigned to Pt(II) species. When the catalyst was used for the hydrodechlorination of CTC, most of the Pt(0) species turned into the Pt(II) species, now located at 73.2 eV. The Pt(II) species could be PtO or $PtCl_2$. It has been reported that the range of binding energy for PtO is 73.9–74.0 eV and that of $PtCl_2$ is 73.2–73.6 eV (30, 31). Therefore, it is concluded that the surface Pt species of the Pt/MgO catalyst working in the hydrodechlorination of CTC is a Pt(II) species with Cl ligands. As mentioned, the presence of Cl on the Pt surface may be responsible for the suppressed H_2 chemisorption at RT over the used catalyst.

Both edge position and white line area of Pt L_{III} XANES shown in Fig. 6 and Table 4 indicate that Pt in the used catalyst has a higher oxidation state than Pt in the fresh catalyst. Even the fresh catalyst showed a higher edge position and a larger white line area compared to those of Pt foil. RSF of the fresh catalyst indicated that this is partly due to the incomplete reduction of Pt because the Pt–Cl interaction was clearly seen in Fig. 8a. The other reason may be due to the small Pt particle size and its interaction with the support (32). For the used catalyst (Fig. 8b) and the deactivated catalyst (Fig. 8c), an additional Pt–O peak appeared. The source of oxygen may be MgO which transforms to $MgCl_2 \cdot xH_2O$ during the hydrodechlorination. Hence, while the surface of Pt in the used Pt/MgO catalyst is mostly the Pt(II)–Cl species, the bulk of the catalyst remained as Pt metal. This explains the fact that Pt particles in Pt/MgO maintain their size and shape as seen in TEM even after the reaction in

spite of the dramatic change in surface state by the reaction as noted by XPS.

CONCLUSIONS

Pt/MgO is an effective catalyst in the selective hydrodechlorination of CTC to $CHCl_3$ with high activity and selectivity. The stable maintenance of the performance is achieved by the proper choice of the reaction conditions, in particular, the reaction temperature and H_2/CTC mole ratio. The reason for the catalyst deactivation is coking of the Pt surface. The active phase of Pt in the Pt/MgO catalyst is Pt metal particles with most of their surface converted to Pt(II)–Cl.

REFERENCES

1. Buchar, N. I., Kuech, T. F., and Scilla, G., *J. Cryst. Growth* **110**, 405 (1991).
2. Tokuda, J., Takai, M., Nakai, H., Gamo, K., and Nawaba, S., *J. Opt. Soc. Am. B* **4**, 267 (1987).
3. Michael, J. V., Lim, K. P., Kumaran, S. S., and Kiefer, J. H., *J. Phys. Chem.* **97**, 1914 (1993).
4. Taylor, P. H., Dellinger, B., and Tirey, D. A., *Int. J. Chem. Kinet.* **23**, 1051 (1991).
5. Windaw, H., and Wyatt, M., *Platinum Met. Rev.* **37**, 186 (1993).
6. Weiss, A. H., Gambhir, B. S., and Leon, R. B., *J. Catal.* **22**, 245 (1971).
7. Helland, B. R., Alvarez, P. J. J., and Schnoor, J. L., *J. Hazard. Mater.* **41**, 205 (1995).
8. Holbrook, M. T., and Harley, D. A., European Patent 0,479,116, A1, 1991.
9. Dogimont, C., Franklin, J., Janssens, F., Schoebrechts, J. P., and Doiceau, G., U.S. Patent 5,146,013, 1992.
10. Miguel, E. T., Gimenez, M. S., Arroyo, A. C., Gomez, L. S., and Martin, A., WO 91/09827, 1991, and U.S. Patent 5,208,393, 1993.
11. Petrosky, J. T., *Vulcan Mater. Com.* U.S. Patent 5,315,050, 1994.
12. Morikawa, S., Yoshitake, M., and Tatematsu, S., Japanese Patents 4-305538, 4-305539, and 4-305540, 1992.
13. Suzuki, T., and Kawaru, S., Japanese Patent 4-364136, 1992.
14. Ollis, D. F., *Environ. Sci. Technol.* **19**, 480 (1985).
15. Choi, W. Y., and Hoffmann, M. R., *Environ. Sci. Technol.* **29**, 1646 (1995).
16. Vance, J. E., and Bauman, W. C., *J. Chem.Phys.* **6**, 811 (1938).
17. Weiss, A. H., Valinski, S., and Antoshin, G. V., *J. Catal.* **74**, 136 (1982).
18. Kim, S. Y., Choi, H. C., Yang, O. B., Lee, K. H., Lee, J. S., and Kim, Y. G., *J. Chem. Soc., Chem. Commun.,* in press.
19. Kim, Y. G., "An Introduction to Chemical Reaction Engineering." Han Rym Won, Seoul, 1990.
20. Rehr, J. J., de Leon, J. M., Zabinsky, S. I., and Albers, R. C., *J. Am. Chem. Soc.* **113**, 5135 (1991).
21. O'Day, P. A., Rehr, J. J., Zabinsky, S. I., and Brown, G. E., *J. Am. Chem. Soc.* **116**, 2938 (1994).
22. Koningsberger, D. C., and Prins, R. (eds.), "X-Ray Absorption: Principles, Applications and Techniques of EXAFS, SEXAFS and XANES." Wiley, New York, 1988.
23. Lytle, F. W., Wei, P. S. P., Greegor, R. B., Via, G. H., and Sinfelt, J. H., *J. Chem. Phys.* **70**, 4849 (1979).
24. Horsley, J. A., *J. Chem. Phys.* **76**, 1451 (1982).
25. Mattheiss, L. F., and Dietz, R. E., *Phys. Rev. B* **22**, 1663 (1980).
26. Teo, B. K., "EXAFS: Basic Principles and Data Analysis." Springer-Verlag, 1986.
27. Bazin, D., Dexpert, H., Bournonville, J. P., and Lynch, J., *J. Catal.* **123**, 86 (1990).
28. Stull, D. R., and Prophet, H., "JANAF Thermochemical Tables," 2nd ed. NSRDS, 1971.
29. Wang, Y. N., Macros, J. A., Simmons, and Klier, K., *J. Phys. Chem.* **94**, 7597 (1990).
30. Moulder, J. F., Stickle, W. F., Sobol, P. E., and Bomben, K. D., "Handbook of X-Ray Photoelectron Spectroscopy." Perkin-Elmer, Minnesota, 1992.
31. Kim, K. S., Winograd, N., and Davis, R. E., *J. Am. Chem. Soc.* **93**, 6296 (1971).
32. Ichkuni, N., and Iwasawa, Y., *Photon Factory Act. Rep.* **9**, 205 (1991).